University of BRISTOL

Peer reviewed version

Link to published version (if available):
10.1002/2016GC006323

Link to publication record in Explore Bristol Research
PDF-document

University of Bristol - Explore Bristol Research
General rights

SHEAR WAVE ANISOTROPY IN NORTHWESTERN SOUTH AMERICA AND ITS LINK TO THE CARIBBEAN AND NAZCA SUBDUCTION GEODYNAMICS

J. Idárraga-García[1], J. -M. Kendall[2], and C. A. Vargas[3]

[1]PhD. Program in Geosciences, Universidad Nacional de Colombia, Bogotá (Colombia).

[2]School of Earth Sciences, University of Bristol, Bristol (United Kingdom).

[3]Department of Geosciences, Universidad Nacional de Colombia, Bogotá (Colombia).

Corresponding author: Javier Idárraga-García (jidarragag@unal.edu.co)

Key Points:

- *S*-wave splitting in northwestern South America shows evidence for several subduction segments with contrasting geodynamics

- *SKS* splitting shows entrained mantle flow beneath subducting slabs, and local *S* splitting is lithosphere-confined

- Results show that seismic anisotropy in northwestern South America is highly controlled by slab tearing structures

Abstract

To investigate the subduction dynamics in northwestern South America, we measured *SKS* and slab-related local *S* splitting at 38 seismic stations. Comparison between the delay times of both phases shows that most of the *SKS* splitting is due to entrained mantle flow beneath the subducting Nazca and Caribbean slabs. On the other hand, the fast polarizations of local *S*-waves are consistently aligned with regional faults, which implies the existence of a lithosphere-confined anisotropy in the overriding plate, and that the mantle wedge is not contributing significantly to the splitting. Also, we identified a clear change in *SKS* fast directions at the trace of the Caldas Tear (~5°N), which represents a variation in the subduction style. To the north of ~5°N fast directions are consistently parallel to the flat subduction of the Caribbean plate-Panama arc beneath South America, while to the south fast polarizations are subparallel to the Nazca-South America subduction direction. A new change in the *SKS* splitting pattern is detected at ~2.8ºN, which is related to another variation in the subduction geometry marked by the presence of a lithosphere-scale tearing structure, named here as Malpelo Tear; in this region, NE-SW-oriented *SKS* fast directions are consistent with the general dip direction of the underthrusting of the Carnegie Ridge beneath South America. Further inland, this NE-SW-trending mantle flow continues beneath the Eastern Cordillera of Colombia and Merida Andes of Venezuela. Finally, our results suggest that the sub-slab mantle flow in northwestern South America is strongly controlled by the presence of lithospheric tearing structures.

1 Introduction

Located in a region where several tectonic plates and minor blocks are interacting through low-(underthrusting) to steep-angle subduction and lithospheric tearing, the northwestern corner of South America offers a relevant natural laboratory to study the deep Earth processes in regions of high tectonic and geodynamic complexity. There are still a number of fundamental unknowns about the tectonic nature of this region, including whether or not the Caribbean Plate subducts beneath northern Colombia and the underlying cause of nests of seismicity across the region. In such subduction systems, the mantle flow-field and state of tectonic stress arise as important mechanisms that are directly related with the surrounding asthenosphere and the overlying continental lithosphere. In this sense, the degree of mechanical coupling between the slabs and the mantle, and between the continental lithosphere and the underlying mantle, is key to obtaining a coherent picture of the geodynamics of the different subduction segments.

Seismic anisotropy, the directional dependence of the seismic waves speed, provides a powerful tool for estimating *in situ* mantle flow pattern, and therefore is a reliable approach to understand past or ongoing deformational processes in the lithosphere-asthenosphere system. Observations of two independent shear waves, or shear wave splitting, provides a robust indicator of such seismic anisotropy. The origin of the seismic anisotropy in the upper mantle has been generally linked to the preferential alignment of olivine crystals under finite strain conditions (LPO: lattice-preferred orientation), whereas in the crust and lithosphere the source of the anisotropy can include LPO, but also the presence of aligned cracks potentially filled with fluid or melt, oriented melt-pockets, or layers of material with contrasting elastic properties (SPO: shape-preferred orientation) [e.g., *Crampin and Booth,* 1985; *Kaneshima and Ando,* 1989; *Kendall,* 1994; *Long and Becker,* 2010; *Long,* 2013]. Under dry mantle conditions, olivine *a*-axes align

parallel to the shear direction, giving rise to A-type LPO fabric [*Mainprice,* 1997; *Mainprice et al.,* 2005].

The study of shear wave splitting provides a direct observation of seismic anisotropy, and is based on the fact that a shear wave propagating through an anisotropic medium splits into two orthogonally polarized quasi-*S* waves travelling at different velocities. The parameters used to describe shear wave splitting, the polarization direction of the fast shear wave (φ) and the cumulative delay time (δt) between the two waves, are measured using three-component seismic waveforms, and provide valuable information about deformation processes. For example, a vertically propagating *S*-wave will be polarized parallel to the mantle flow direction in the presence of A-type LPO mantle fabric [*Mainprice and Silver,* 1993].

In this paper we estimate shear wave splitting parameters from teleseismic *SKS* and local, subduction-related *S* phases arriving at broadband seismic stations of the Colombian National Seismological Network (CNSN), and some stations of the Global Seismographic Network (GSN) located in Panama, northern Ecuador and western Venezuela. Our aim is to investigate the seismic anisotropy structure and its link to the geodynamics of the Nazca and Caribbean subduction systems in northwestern South America.

2 Subduction Systems in Northwestern South America

The study zone is located in the northwestern corner of South America and includes Colombian territory and adjacent areas (Figure 1). In this area the geologic and tectonic framework is complex due to the convergence of three major tectonic plates (South American, Nazca and the Caribbean) and a number of minor tectonic blocks (Panama Arc, North Andes and Maracaibo blocks) [*Taboada et al.,* 2000; *Vargas and Mann,* 2013] (Figure 1). The current state is that the oceanic lithosphere of the Nazca Plate is subducting beneath continental South American plate with a dip angle varying between 30° and 40° [*Trenkamp et al.,* 2002; *Vargas and Mann,* 2013]. In contrast, the interaction between the South American and Caribbean Plates is much more controversial, and has been the subject of heated debate for the last several years. Some authors have argued that the oceanic Caribbean slab is subducting under the South American Plate at a very low angle [e.g., *Pennington,* 1981; *van der Hilst and Mann,* 1994; *Taboada et al.,* 2000; *Vargas and Mann,* 2013; *Bernal-Olaya et al.,* 2015], while other authors have proposed that the boundary between these two plates corresponds to a 100 km wide active transpressional zone [e.g., *Audemard,* 1993].

The geometry and dynamics of the subducting slabs in northwestern South America has been addressed by the analysis of the distribution of shallow to intermediate seismicity and focal mechanisms [*Pennington,* 1981; *Gutscher et al.,* 1999; *Cortés and Angelier,* 2005; *Bernal-Olaya et al.,* 2015], and by the study of seismic tomographic images [*van der Hilst and Mann,* 1994; *Gutscher et al.,* 2000; *Taboada et al.,* 2000; *Vargas and Mann,* 2013; *Bernal-Olaya et al.,* 2015]. In general, these investigations have highlighted the presence of the flat subducting slab of the Caribbean plate (without subduction-related volcanism), in contrast to the steeper dipping slab of the Nazca Plate, which is associated with an active volcanic arc. Recently, *Vargas and Mann* [2013] presented two regional lithospheric cross sections in northwestern South America obtained from relocated earthquake hypocentral solutions, models supported by gravity and magnetic data, and coda-Q (Q_c) tomography. Their results have shown evidence for a

lithospheric tear zone where the Panama Arc collides with northwestern Colombia. This mega-structure, called the Caldas Tear, extends for approximately 240 km with general orientation E-W (Figure 1), and appears to represent the boundary between a low-angle (20°-30°) subduction zone in northern Colombian Caribbean region, called the Bucaramanga Segment [*Pennington,* 1981], which is not associated with subduction-related volcanism, and a steep-angle (30°-40°) subduction zone located in southwestern Colombia, named Cauca Segment [*Pennington,* 1981], that is related to an active volcanic chain [*Vargas and Mann,* 2013]. The Caldas tear is collinear with the 9-12 Ma, E-W oriented Sandra oceanic ridge on the unsubducted portion of the Nazca plate to the west, and may also represent the southern boundary of the Panama Arc indenter, which corresponds to an extinct island arc that began subducting beneath northwestern South America around 12 Ma. Regarding its origin, the aforementioned authors proposed that the Caldas tear may have formed as a zone of lithospheric weakness along the now subducted part of the Sandra spreading ridge.
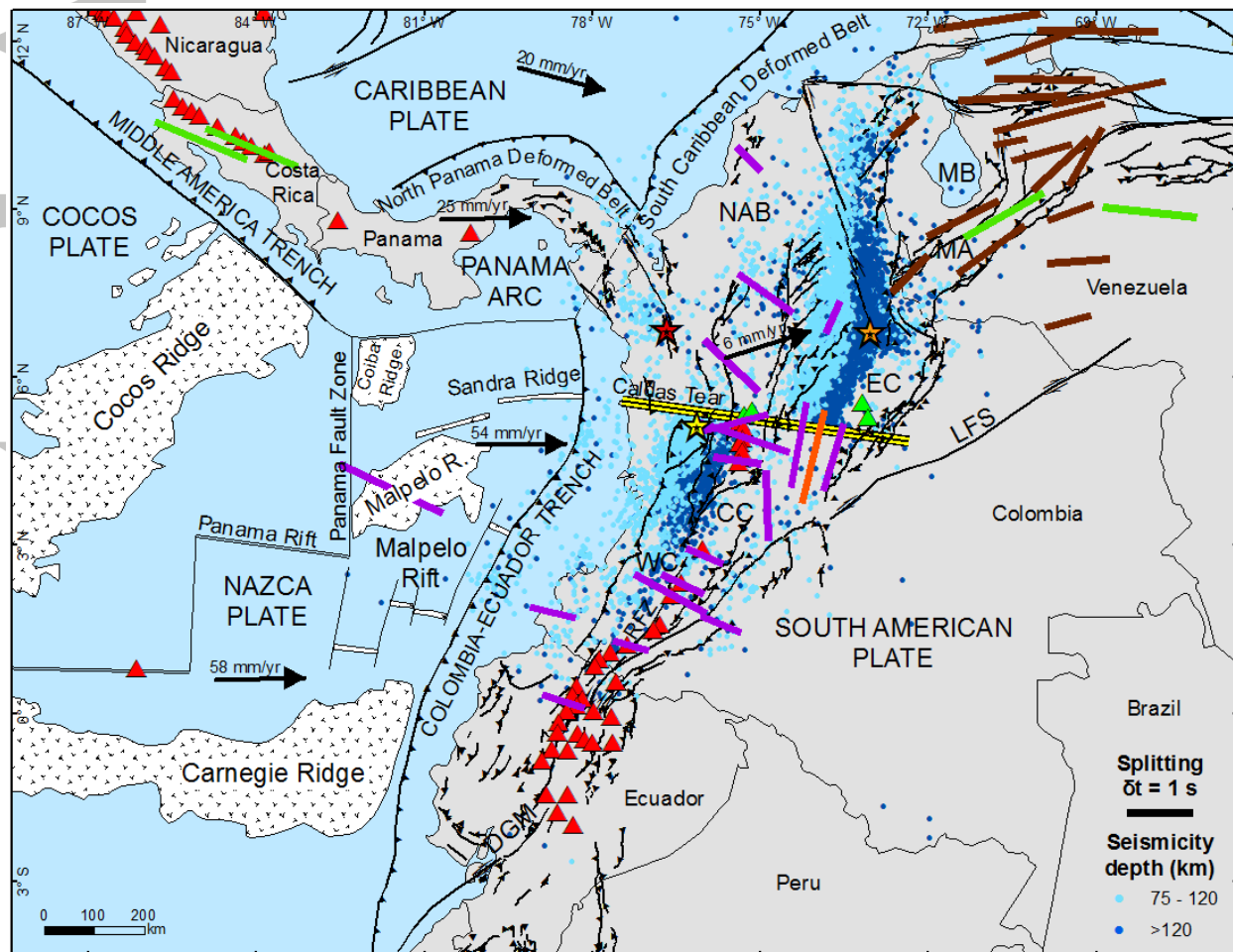
Figure 1. Tectonic setting of northwestern South America showing major tectonic plates and blocks boundaries, oceanic ridges and rifts, regional fault systems, volcanoes (active: red triangles; inactive: green triangles), GPS vectors [from *Trenkamp et al.,* 2002], and the intermediate-to-deep instrumental seismicity recorded by the Colombian National Seismological Network. The proposed trace of the Caldas Tear (thick yellow-black line) is related to the right-lateral offset of the intermediate-to-deep seismicity, the sudden termination of the active volcanism, and the presence of two different subduction segments to the north (Bucaramanga segment) and to the

south (Cauca segment). Stars represent the location of seismic nests (red: Murindo seismic nest; Orange: Bucaramanga seismic nest; yellow: Cauca seismic nest). Previous splitting measurements are taken from *Wüstefeld et al.* [2009], and include results from *Russo and Silver* [1994] (red bars), *Piñero-Feliciangeli and Kendall* [2008] (green bars), *Masy et al.* [2011] (brown bars), and *Porritt et al.* [2014] (purple bars). NAB: North Andes Block; MB: Maracaibo Block; LFS: Llanos Fault System; DGM: Dolores-Guayaquil Megashear; RFZ: Romeral Fault Zone; MA: Merida Andes; WC: Western Cordillera; CC: Central Cordillera; EC: Eastern Cordillera.

Gutscher et al. [1999] proposed the existence of four segments on the subducting Nazca plate beneath the northern Andes. The first segment, located between 6ºN and 2.5ºN, exhibits a steep ESE-dipping subduction and it is associated with a narrow volcanic chain; this segment would correspond to *Pennington´s* [1981] Cauca Segment. The second segment, from 2.5ºN to 1ºS, is linked to the subduction of the Carnegie Ridge and shows an intermediate-depth seismic gap and a broad volcanic arc. The third segment, which correlates to *Pennington´s* [1981] Ecuador Segment, is located between 1ºS and 2ºS, and it is related to a steep NE-dipping subduction and a narrow volcanic arc; finally, the fourth segment, south of 2ºS shows a flat subduction and absence of a modern volcanic chain.

Three earthquake nests of intermediate depth are present beneath the northern Andes, the tectonic interpretation of which has not yet reached a clear consensus (Figure 1). The Bucaramanga seismic nest (BN) is located at a depth of ~160 km and has a volume of approximately 13 x 18 x 12 km [*Schneider et al.,* 1987; *Frohlich et al.,* 1995]. Some interpretations regarding its origin include: a contact or overlap zone between Caribbean and Nazca slabs [*van der Hilst and Mann,* 1994], extreme bending of the Caribbean slab [*Taboada et al.,* 2000; *Cortés and Angelier,* 2005; *Vargas and Mann,* 2013], and the southern termination of Caribbean plate [*Corredor,* 2003]. The Cauca seismic nest (CN) is located ~400 km southwest of the BN and lies beneath the Romeral fault zone along the northern edge of Cauca valley. *Cortes and Angelier* [2005] proposed that the stress pattern related to the CN is compatible with a model of a down-dip broken slab due to gravitational drag of the plunging slab of the current Nazca plate; *Vargas and Mann* [2013] suggested an alternative hypothesis in which the CN would be the combined product of eastward decoupling of plates along the Caldas Tear and flexion processes of the plate during subduction. The third earthquake nest, called the Murindo seismic nest is located near to the Panama and Colombia border, and correspond to intermediate depth seismicity associated with the proximal compressed stress response to the indentation of the Panama arc against northwestern South America.

On the other hand, some regional compilations of GPS data provide further and more quantitative insights into the tectonic setting of northwestern South America (Figure 1). The measurements from CASA GPS project show that relatively fast subduction of the Nazca plate is currently ongoing along the Colombia-Ecuador trench, with a convergence rate of 54-58±2 mm/yr [*Trenkamp et al.,* 2002]. Also, GPS vectors in western Colombia exhibit a remarkable decrease in velocities, which is consistent with the current collision of the Panama arc with the northwestern South America at a rate of 25 mm/year along a N-S trending suture near the Panama-Colombia border [*Trenkamp et al.,* 2002]. CASA GPS results show an E-SE oriented oblique convergence of 20±2 mm/yr between Caribbean and South American plates, and a convergence of 7±2 mm/yr toward SW between the Caribbean plate and Panama arc [*Trenkamp et al.,* 2002]. Finally, the North Andes Block is escaping to the northeast at a rate of 6±2 mm/year [*Trenkamp et al.,* 2002].

3 Previous Studies of Seismic Anisotropy in Northwestern South America

There are relatively few investigations on the seismic anisotropy involving northwestern South America and Caribbean region.

Using earthquake data recorded by a temporary deployment of 9 seismometers in northeastern Colombia, *Shih et al.* [1991] investigated the seismic anisotropy above the Bucaramanga seismic nest. They interpreted the shear wave splitting observed in terms of the alignment of olivine and orthopyroxene crystals as a product of the shearing associated with the subduction, aided by fluids migrating from the subducting plate when the slab exceeds 100 km in depth.

Russo and Silver [1994] described the anisotropy and strain field of the mantle beneath Nazca plate, Cocos plate and Caribbean region from shear wave splitting of *S* and *SKS* phases. They found evidence for horizontal trench-parallel flow in the mantle beneath the subducting Nazca plate along much of the Andean subduction zone. The explanations to this flow include retrograde motion of the slab, the decoupling of the slab and underlying mantle, and a partial barrier to flow at depth.

In northwestern South America and Caribbean region, *Piñero-Feliciangeli and Kendall* [2008] identified sub-slab mantle flow parallel to the Caribbean plate boundaries. Furthermore, they concluded, from the analyses of local splitting, that most of the upper mantle wedge is isotropic, and the splitting of the local *S* phases occurs mostly in the crust and uppermost mantle.

Masy et al. [2011] measured shear wave splitting across the Merida Andes in western Venezuela and found evidence for a trench-parallel mantle flow passing around the northwest corner of the Caribbean plate and along the northern edge of South America. Also, their results suggest that the seismic anisotropy beneath the Merida Andes is probably related to lithospheric deformation.

Recently, *Porritt et al.* [2014] used data from the Colombian National Seismological Network to investigate the seismic anisotropy and slab dynamics from *SKS* splitting measurements in Colombia. Their results show trench-perpendicular fast polarizations in the stations close to the Colombia-Ecuador trench, which farther to the east, in the back-arc region, abruptly change to trench-parallel anisotropy. According to the authors, the rotation in the fast directions could be related to a lithospheric signature, or asthenospheric flow through the Caldas Tear.

4 Data and Methodology

We analyzed the shear wave splitting of two different shear phases, core refracted *SKS* and local subduction-related *S,* to improve the spatial resolution of the anisotropic structure in the northern South America. Most of the data used in this study were provided by the Colombian National Seismological Network (CNSN), which is operated by the Geological Survey of Colombia, and encompassed five years of information (2008-2012), although some events between 2013 and 2015 were included in the database as well. Also, we used data from some stations of the Global

Seismographic Network (GSN) located in Panama, northern Ecuador, and western Venezuela. In total, we obtained shear wave splitting results for 35 stations (30 in Colombia, 2 in Panama, 2 in Ecuador, and 1 in Venezuela) for the *SKS* phase, and 16 stations (all of them in Colombia) for the local *S* phase (Table 1).

Table 1. List of the stations with at least one good result of shear wave splitting. CNSN: Colombian National Seismological Network; GSN: Global Seismographic Network

STATION	LATITUDE	LONGITUDE	SPLITTING RESULT	NETWORK	NUMBER AS SHOWN IN FIGURES 4 AND 5
ANIL	4,49	-75,40	*SKS*, local *S*	CNSN	21
AZU	7,79	-80,27	*SKS*	GSN	3
BCIP	9,17	-79,84	*SKS*	GSN	2
BRR	7,10	-73,71	*SKS*, local *S*	CNSN	12
BRUN	-1,42	-78,41	*SKS*	GSN	35
COD	9,93	-73,44	Local *S*	CNSN	37
CAP2	8,64	-77,36	*SKS*	CNSN	4
CHI	4,63	-73,73	*SKS*	CNSN	23
FLO2	1,58	-75,65	*SKS*	CNSN	31
GCUF	1,23	-77,34	*SKS*	CNSN	30
GUY	5,22	-75,39	*SKS*	CNSN	18
HEL	6,19	-75,52	*SKS*	CNSN	14
MARA	2,84	-75,95	*SKS*	CNSN	26
MON	8,77	-75,66	*SKS*	CNSN	5
NOR	5,56	-74,86	*SKS*, local *S*	CNSN	15
OCA	8,23	-73,31	*SKS*, local *S*	CNSN	8
OTAV	0,23	-78,45	*SKS*	GSN	33
PAL	4,90	-76,28	*SKS*, local *S*	CNSN	20
PCON	2,32	-76,39	*SKS*, local *S*	CNSN	28
POP2	2,54	-76,67	*SKS*, local *S*	CNSN	27
PRA	3,71	-74,88	*SKS*	CNSN	25
PRV	13,37	-81,36	*SKS*	CNSN	1
PTB	6,54	-74,45	*SKS*, local *S*	CNSN	13
PTLC	-0,17	-74,79	*SKS*	CNSN	34
ROSC	4,84	-74,32	*SKS*, local *S*	CNSN	22
RREF	4,90	-75,34	*SKS*	CNSN	19
RUS	5,89	-73,08	*SKS*, local *S*	CNSN	16
SDV	8,88	-70,63	*SKS*	GSN	9
SJC	9,89	-75,18	*SKS*	CNSN	6
SMAR	11,16	-74,22	*SKS*	CNSN	7
SML	8,80	-74,07	Local *S*	CNSN	38
SOTA	2,13	-76,60	*SKS*, local *S*	CNSN	29
TAM	6,43	-71,79	*SKS*, local *S*	CNSN	17

TUM	1,82	-78,72	*SKS*	CNSN	32
URE	7,75	-75,53	*SKS*	CNSN	11
URI	11,70	-71,99	Local *S*	CNSN	36
YOT	3,98	-76,34	*SKS*, local *S*	CNSN	24
ZAR	7,49	-74,85	*SKS*	CNSN	10

For the *SKS* splitting analysis we used teleseismic events with epicentral distances between 85° and 130°, and magnitudes larger than M5. Subduction-related local events were selected with depths greater than 70 km to ensure that the *S* waves have sampled the supra-slab mantle and crust and with raypaths arriving with incident angles less than 35° to avoid phase conversions at the surface (Figure 2). Most of these events originated in the Bucaramanga and Cauca seismic nests. Prior to the splitting analysis, data were filtered using Butterworth bandpass filters with corner frequencies between 0.04 and 0.3 Hz in the case of the teleseismic events (*SKS*), and between 0.1 and 2 Hz for local earthquakes, to improve the signal-to-noise ratio on each seismogram.
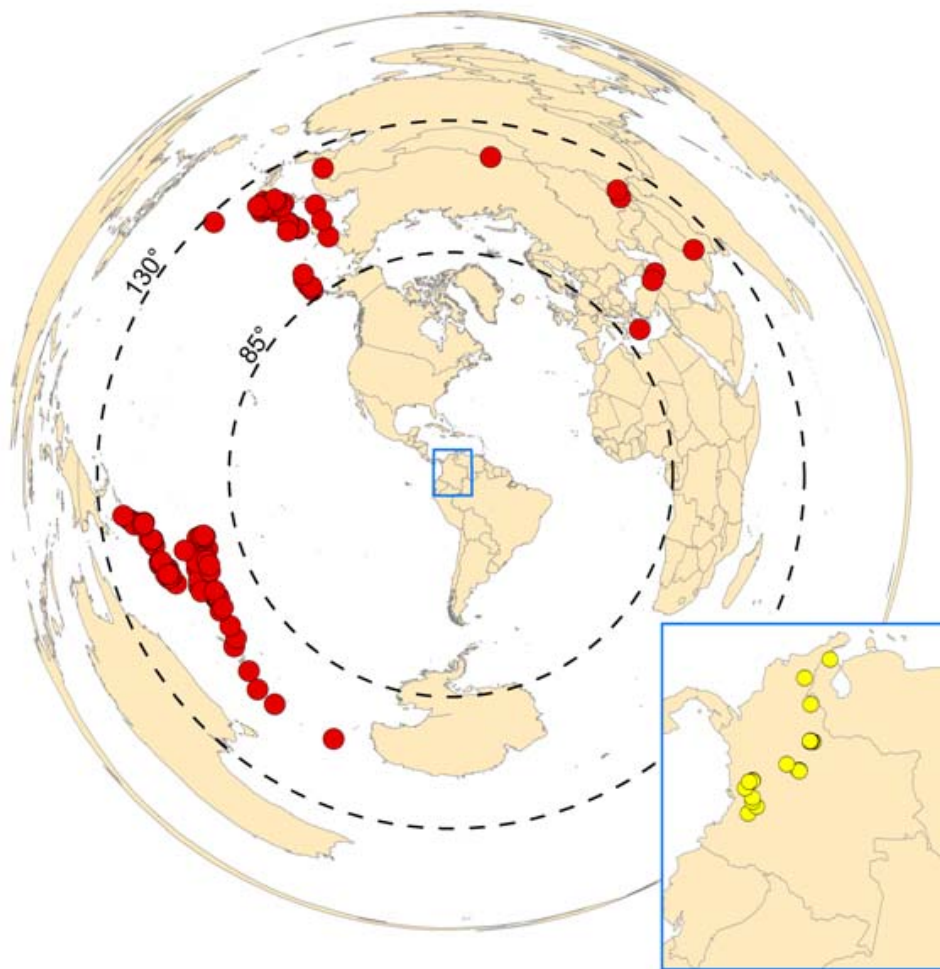

Figure 2. Epicentral distribution of the teleseismic (red dots) and local (yellow dots) earthquakes which produced good *SKS* and local *S* splitting measurements, respectively.

We estimated shear wave splitting parameters, the polarization of the fast shear wave (φ) and delay time (δt), from three-component seismic waveforms using the eigenvalue minimization method of *Silver and Chan* [1991]. This method finds the splitting parameters that best linearize the *S*-wave particle motion, or, put another way, minimize the second eigenvalue of the covariance matrix of the horizontal components in a time window around the *S* (*SKS*, *SKKS*, etc.) arrival. An initially linearly polarized shear-wave in an isotropic medium will split into two orthogonally polarized shear waves when passing through an anisotropic medium. This leads to a characteristic elliptical particle motion if the seismic wavelength is larger than the delay time, which is usually the case. Furthermore, the presence of energy on the component orthogonal to the polarization of the initial shear wave is another indicator of shear wave splitting. As *SKS* is polarized in the radial plane at the core-mantle boundary, the presence of energy on the transverse component is also an indicator shear-wave splitting in *SKS* phases. The method grid-searches for all possible values of φ and δt, rotates and time-shifts the horizontal components, until the second eigenvalue is minimized. This also reveals the initial source polarization of the *S* wave. The grid-search is used to produce a contour plot of the energy of the second eigenvalue for each fast direction-delay time pair. An f-test is used to find the best-fitting splitting parameters, which correspond to the minimum on this contour plot, and the 95% confidence region around this point provides an assessment of the errors in these parameters [*Silver and Chan,* 1991].

In order to remove the subjectivity related to the choice of the shear wave analysis window, we used the cluster analysis method proposed by *Teanby et al.* [2004]. Also, we visually checked all the splitting measurements and performed a quality control with the inclusion of some qualitative and quantitative conditions. Qualitative conditions included the observation of minimal energy on the corrected transverse component and linearization of the original elliptical particle motion after the removal of the splitting effects; quantitative conditions included errors (reported here as one-sigma errors) less than 25º in φ and less than 1 s in δt for the *SKS* wave, and 0.5 seconds for the local *S*-wave phases. Furthermore, we reject any *SKS* splitting measurements where the estimate of the source polarization is greater than 25 degrees from the backazimuth directions. Figure 3 shows an example of well-constrained shear wave splitting result for both *SKS* and local *S* phase.

Variations of the splitting parameters (φ and δt) with the azimuth are evidence of the presence of complex anisotropy beneath the station, such as sharp lateral variations in anisotropy [*Hammond et al.,* 2010], dipping anisotropic layers [*Levin and Park,* 1998] or multiple anisotropic layers [*Savage,* 1999]. In this study we did not find any strong evidence of backazimuthal variations in the splitting parameters, although it should be noted that our backazimuthal coverage was poor (Figure 2). For example, most of the stations with at least five reliable *SKS* splitting measurements achieved seismic rays only coming from one backazimuthal quadrant, and a very few stations with coverage in two quadrants (Figure S2). Consequently, we proceeded to stack the error surfaces of the splitting measurements in each single station in order to report the "mean" splitting parameters using the approach of *Restivo and Helffrich* [1999].
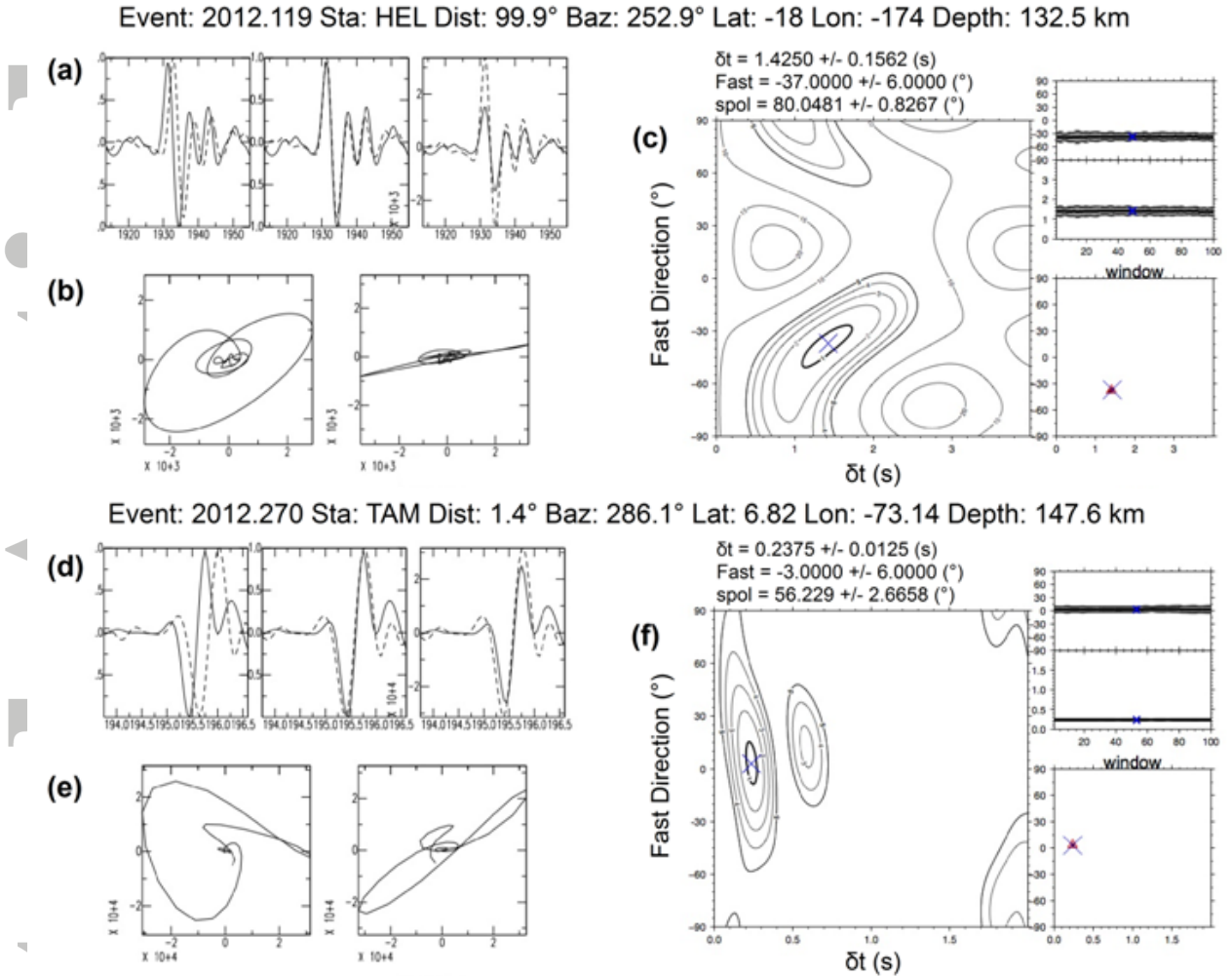
Figure 3. Example of two shear wave splitting measurements using the method of *Silver and Chan* [1991] and *Teanby et al.* [2004]. Top: *SKS* splitting result for station HEL (panels a, b and c). Bottom: Local *S* wave splitting result for station TAM (panels d, e and f). (a and d) Fast and slow waveforms for uncorrected (left) and corrected (middle: normalized; right: actual amplitudes) seismograms. (b and e) Particle motion before (left) and after (right) correction. A well-constrained result exhibits elliptical particle motion before and linear particle motion after correction for splitting. (c and f) Results of grid-search over fast direction (φ) and delay time (δt). The optimal φ and δt pair (blue cross) is that which linearizes the particle motion, and the first surrounding contour marks the 95% confidence region. The far right boxes show the result of the cluster analysis [*Teanby et al.,* 2004] – the top shows how the splitting parameters vary with a window around the shear phase, and the lower shows the best cluster in these results. Both examples show a very stable estimate of δt and φ, as only one cluster is visible.

5 Shear-Wave Splitting Observations

Our results indicate that significant shear wave splitting is present along the northwestern corner of South America. We obtained 257 high-quality splitting measurements from teleseismic *SKS* phases arriving at 35 seismic stations, and 85 splitting results of local *S* phases arriving at 16 seismic stations (Table 2 shows the stacked results, and Table S1 in the Supporting Information includes the individual measurements at each station).

Table 2. List of the high-quality, stacked splitting results obtained from teleseismic *SKS* and local *S* phases.

STATION	STACKED *SKS* SPLITTING		NUMBER OF MEASUREMENTS	STACKED LOCAL *S* SPLITTING		NUMBER OF MEASUREMENTS
	φ	δt		φ	δt	
ANIL	273	1.07	11	0	0.63	1
AZU	84	0.94	3	-	-	0
BCIP	79	0.30	4	-	-	0
BRR	335	1.45	5	27	0.12	24
BRUN	12	0.66	8	-	-	0
COD	-	-	0	107	0.11	1
CAP2	321	0.82	4	-	-	0
CHI	18	1.37	5	-	-	0
FLO2	82	1.02	19	-	-	0
GCUF	283	0.70	10	-	-	0
GUY	297	1.27	1	-	-	0
HEL	316	1,30	43	-	-	0
MARA	333	0.67	11	-	-	0
MON	296	0.80	9	-	-	0
NOR	311	0.72	2	173	0.21	5
OCA	350	0.87	5	11	0.36	2
OTAV	62	2.37	8	-	-	0
PAL	302	0.90	4	38	0.18	2
PCON	283	0.92	11	154	0.62	1
POP2	336	1.32	11	243	0.26	4
PRA	274	0.70	2	-	-	0
PRV	331	1.60	3	-	-	0
PTB	313	2.17	5	156	0.20	8
PTLC	290	1.47	2	-	-	0
ROSC	19	1.02	4	66	0.60	1
RREF	86	2.50	16	-	-	0
RUS	59	1.45	2	163	0.42	12
SDV	55	1.02	12	-	-	0
SJC	320	0.65	6	-	-	0
SMAR	323	0.75	2	-	-	0
SML	-	-	0	19	0.16	1
SOTA	36	0.75	2	21	0.46	1
TAM	50	1.70	3	11	0.26	20
TUM	67	1.97	2	-	-	0
URE	319	1.90	1	-	-	0
URI	-	-	0	15	0.23	1
YOT	66	0.47	4	63	0.16	1
ZAR	304	0.70	17	-	-	0

5.1 *SKS* Splitting

Figure S1 shows that stations AZU, BRR, CAP2, CHI, HEL, PTLC, PRA, RUS, SOTA, TAM, TUM and YOT present very constant φ values, with a variation less than 45° between individual measurements. On the other hand, other stations with two or more reliable *SKS* splitting results exhibit some scatter in their fast directions. However, in this case, most of the individual measurements at each of these stations are grouped into a clear dominant tendency, with just one or two individual values out of this trend (for example, stations ANIL, BCIP, BRUN, FLO2, GCUF, MARA, MON, NOR, OCA, OTAV, PAL, PCON, POP2, PRV, PTB, ROSC, RREF, SDV, SJC, SMAR, and ZAR in Figure S1). This observation suggests that a complex anisotropic structure could be present beneath those stations, which could be addressed through the analysis of the splitting parameters variation (φ and δt) with the backazimuth. In our study zone, as it is for the rest of South America, there is a relatively limited backazimuthal distribution of seismic events in the epicentral range of *SKS* phase analysis (Figure 2). The backazimuthal coverage at stations with five or more *SKS* splitting measurements is quite limited, with most stations only achieving coverage in the southwestern backazimuthal quadrant, only a few stations with coverage in two quadrants, and none with coverage in three or more quadrants. In the case of stations having coverage in two quadrants, a number of them insinuate that some variation of the splitting parameters with the station-to-source backazimuth could be present (Figure S2), but it is difficult to get a clear conclusion about the presence or not of multi-layer anisotropy given the restricted range of backazimuths.

According to the above, we proceeded to estimate the average values of the *SKS* splitting parameters at each station using the method of *Restivo and Helffrich* [1999]. Figure 4 shows the general picture of the stacked *SKS* splitting patterns obtained in this study. If we compare our results with those from Porritt et al. [2014] in the 17 seismic stations that are common in both studies, it can be seen that the average fast directions are very similar, but our delay times are consistently larger in most cases. According to the patterns, four regions of contrasting *SKS* splitting can be differentiated:

Region I, located north of ~5°N and west of ~-73°W, encompasses northwestern Colombia and Panama. The fast directions show a dominant NW-SE orientation (azimuths ranging between 296° and 350°) for the stations located in Colombia (NOR, HEL, PTB, BRR, OCA, ZAR, URE, MON, CAP2, SJC, SMAR, and PRV), and a nearly E-W trending (azimuths of 84° and 79°) for the stations located in Panama (BCIP and AZU). These two orientations (NW-SE and E-W) are closely parallel to the direction of convergence of the Caribbean plate and Panama arc respectively against the northwestern corner of South America. Delay times vary between 0.65 and 2.17 s, but with ~60% of the measurements falling in the range of 0.65-0.87 s. The smallest lag times (<1 s) are concentrated north of ~7.8°N (stations CAP2, SMAR, MON, SJC, OCA, BCIP, and AZU) (Figure 4).

Region II includes the zone west of the Eastern Cordillera of Colombia, between ~5°N and ~2.8°N. Here, the *SKS* fast directions vary between 66° and 302°, and are roughly parallel-subparallel to the average convergence direction between the Nazca and South American plates. Delay times are pretty variable, with values between 0.47 and 2.50 s; the largest δt values (>1 s)

are observed at the stations located in the Central Cordillera of Colombia (GUY, RREF, and ANIL), whereas the smallest values are reported at the stations located in the valleys between the mountain ranges (YOT and PRA) (Figure 4).

Region III spans from ~2.8ºN to ~2ºS, and covers southwestern Colombia and northern Ecuador. Here, the behavior of the results is more complex than those of the Regions I and II, showing a variety in the patterns of the fast orientations and lag times (Figure 4). Five of the stations (FLO2, MARA, OTAV, POP2, and TUM) reported trench-oblique (azimuths between 242° and 336°) *SKS* fast directions, three stations (GCUF, PTLC, and PCON) nearly trench-perpendicular tendencies (azimuths between 266° and 290°), and two stations (SOTA and BRUN) parallel-trench (azimuths of 12° y 36°) behaviors. Delay times range between 0.66 and 2.37 s, but ~60% of the results are ≤1.0 s (Figure 4).

Region IV is restricted to the Eastern Cordillera of Colombia north of ~4.5°N and the Merida Andes in Venezuela. *SKS* splitting patterns here are highly contrasting with the results previously described for Regions I, II and III, mainly with regard to the fast component orientation. Stations ROSC and CHI show φ values striking NNE-SSW (azimuths of 18° and 19° respectively), which change to a more NE-SW trending to the northeast beneath stations RUS, TAM and SDV (azimuths of 59°, 50° and 55°, respectively). δt values are pretty constant, ranging between 1.02 and 1.7 s (Figure 4).

Figure 4. Stacked *SKS* shear wave splitting at each station (numbers correspond to those listed in Table 1). Orientation of the thin blue bars indicate fast component polarization direction (φ) and the bar length is proportional to delay time (δt). Note the change in the dominant trend in φ at ~5°N (Regions I and II) and at ~2.8°N (Regions II and III). Fast orientations also exhibit different trends at stations in Eastern Cordillera and Merida Andes (Region IV). Red box indicates the area shown in Figure 7. Profiles AA' and BB' are shown in Figure 9. NAB: North Andes Block; MB: Maracaibo Block; LFS: Llanos Fault System; DGM: Dolores-Guayaquil Megashear; RFZ: Romeral Fault Zone; MA: Merida Andes; WC: Western Cordillera; CC: Central Cordillera; EC: Eastern Cordillera; CR: Coiba Ridge; SR: Sandra Ridge; MR: Malpelo Ridge; MRf: Malpelo Rift; CgR: Carnegie Ridge. Inset map shows the four regions differentiated based on the *SKS* splitting behavior.

5.2 Local *S* Splitting

We were able to obtain reliable results of local *S* splitting at 16 stations along the study zone (13 of these stations also with *SKS* results). Compared to the *SKS* splitting results, the fast directions of the local *S* splitting are more constant in their behavior between individual measurements, with φ values showing clearly dominant trends in all stations (Figure S3). The stacked patterns of the corresponding splitting parameters are shown in Figure 5.
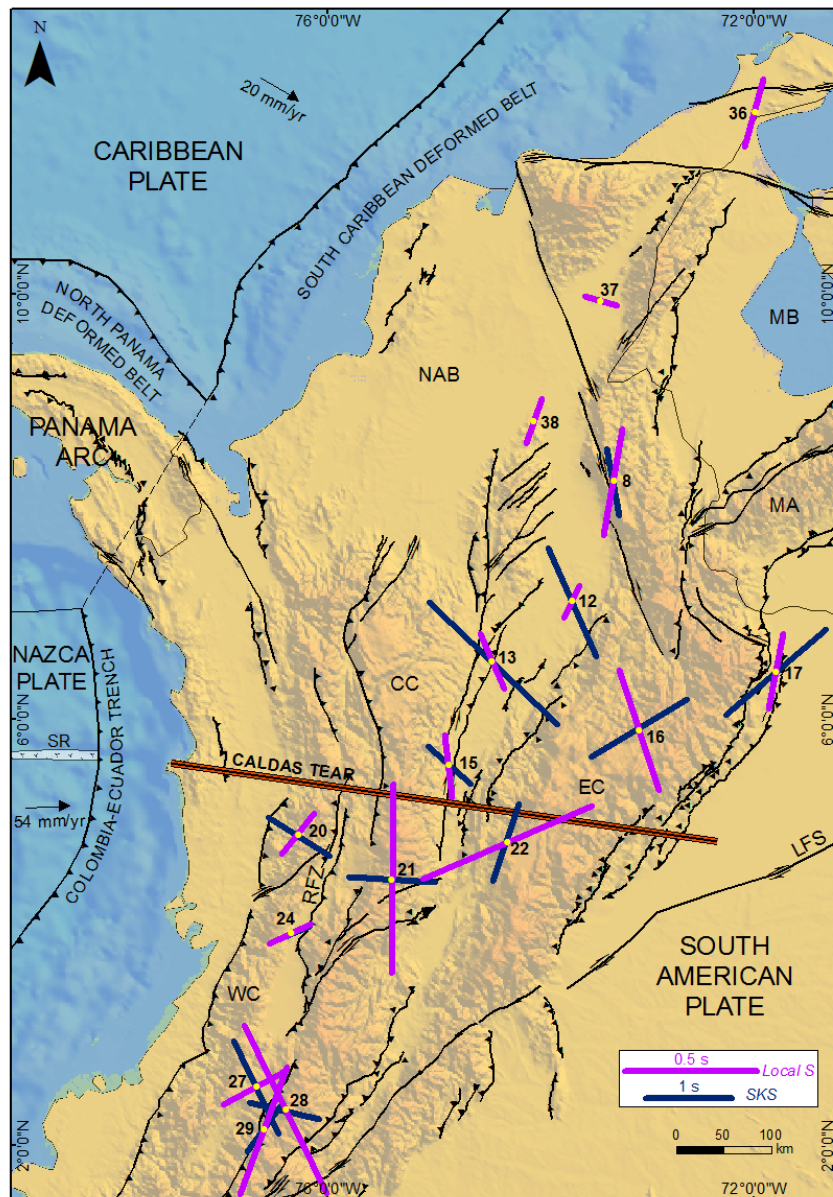

Figure 5. Stacked local *S* wave splitting patterns (magenta bars) obtained at 16 stations (numbers correspond to those listed in Table 1). We also include the stacked *SKS* splitting results (blue bars) to facilitate the comparison. Orientation of the bars indicate fast component direction (φ) and the bar length is proportional to delay time (δt). Local *S* and *SKS* splitting behavior are highly contrasting at most stations. Also, local *S* fast directions are consistently aligned with some major regional-scale fault systems. Abbreviations are the same as shown in Figure 4.

Fast directions are grouped into two preferred orientations: one ranges from N-S to NE-SW (azimuths between 0° and 66°) and it is observed at 11 stations (ANIL, OCA, TAM, URI, SML, SOTA, BRR, PAL, POP2, YOT, and ROSC); the second φ trend is NW-SE (azimuths between 107° and 173°) at stations COD, PCON, PTB, RUS, and NOR. A common observation in most stations is that the fast orientations are quite different from those of *SKS* phase. In fact, in stations as ANIL, RUS, and PAL the difference between the two φ values is close to 90°. It is also striking that the local *S* fast directions are consistently aligned with some crustal-scale fault zones. On the other hand, δt values are typically small, ranging between 0.11 and 0.63 s (~81% less than 0.46 s), and significantly smaller than their *SKS* counterparts (Figure 6).

6 Discussion

6.1 Constraining the Depth to the Anisotropic Structure: *SKS* vs Local *S* Splitting

One of the disadvantages of the shear wave splitting method lies in the fact that is a path-integrated measurement, therefore its depth (vertical) resolution is poor. This means that the *SKS* phase splitting could be the product of the anisotropy present anywhere along its path from the core-mantle boundary to the station on surface. Based on arguments of the size of Fresnel zones, sharp lateral variations on short length scales argue for a more shallow origin to the differences in anisotropy [*Alsina and Sneider,* 1995; *Hammond et al.,* 2010[. Furthermore, this drawback is also addressed with the use of several seismic phases with different raypaths (e.g., different depths) [e.g., *Di Leo et al.,* 2012].

From the analysis of *SKS* splitting beneath Colombia, *Porrit et al.* [2014] propose that much of the measured anisotropy could be related to azimuthal anisotropy in the mantle wedge, with a smaller contribution from the subslab uppermost mantle. In this study, we compare the results of teleseismic *SKS* with local *S* phase splitting to obtain a better vertical resolution of the anisotropic fabrics associated with the subduction processes. The local, subduction-related earthquakes analyzed are located between 78 and 110 km depth, and were likely originated close to the top of the subducting slab. Therefore, the *S* phase traveled directly from the source to the recording station at surface, sampling some portion of the descending slab, mantle wedge and continental lithosphere. Although it was only possible to obtain high-quality local *S* splitting results at 16 stations, some important observations can be raised about the depth distribution of the anisotropic signal.

As it can be seen in Figures 5 and 6, the delay times obtained from the local *S* splitting are small, varying between 0.64 (station ANIL) and 0.11 s (station COD). The average δt value is 0.31 s. These lag times are clearly smaller than those obtained for the *SKS* phase, which range between 0.47 (station YOT) and 2.17 s (station PTB), with an average value of 1.14 s (Figure 6). These observations lead to the conclusion that most of the splitting of the *SKS* is the result of the anisotropic structure present in the upper mantle beneath the downgoing slabs, although we cannot rule out some contributions from deeper parts of the mantle (transition zone, lower mantle and *D''* layer). Also, it could be the response of some contribution from the subducted oceanic lithosphere itself. In this scenario, if both δt mean values are sufficiently representative, we could suggest that about 0.83 s (of 1.14 s) of the delay between the *SKS* fast and slow components is related to active flow processes in the mantle beneath the subducting slabs. The extension in

depth of this anisotropic layer within the sub-slab mantle depends upon the anisotropy percentage, which has been estimated to be ~3.7% in others regions of the world from petrographic measurements [*Mainprice and Silver,* 1993]. According to this, it would be necessary the presence of a ~100 km thick mantle layer beneath the descending slabs with 3.7% of anisotropy to produce 0.83 s of *SKS* splitting (assuming a mean shear-wave velocity of 4.5 km/s).
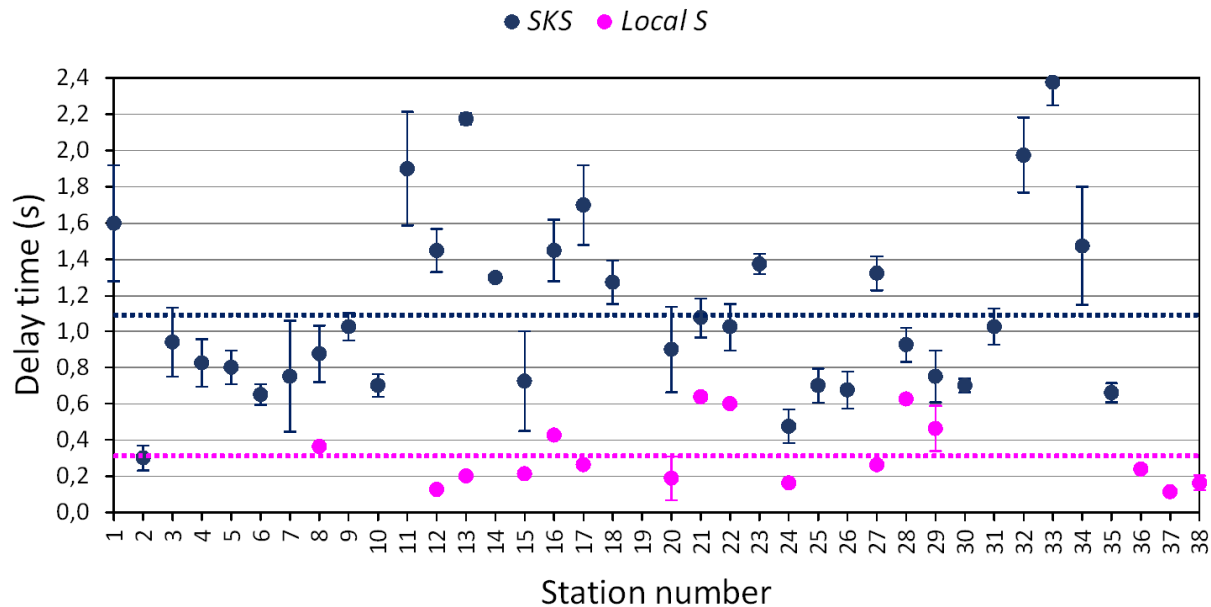

Figure 6. Comparison between the *SKS* and local *S* splitting delay times (*δt*). Dotted lines represent the delay time mean values of each seismic phase. Station numbers correspond to those listed in Table 1.

As mentioned above, the local *S* spitting observed could be the cumulative effect of the anisotropic structure present in the subducting slabs, mantle wedge and continental lithosphere. The observation that most of the *S*-wave fast directions are aligned parallel-subparallel to several regional-scale fault systems (Figure 5) could lead us to the assumption that the local *S* splitting is mainly confined to the continental crust. The range of delay times (0.11-0.64 s) also supports a crust-related seismic anisotropy, as has been previously reported in stations located above fault zones [*Savage et al.,* 1990].

The crustal thickness reported beneath the stations with local *S* splitting results range between 27 and 63 km (Table 3), with the maximum values observed in sectors of the Central and Eastern Cordilleras of Colombia [*Poveda et al.,* 2015]. Taking an average crustal shear wave velocity of 3.6 km/s, and assuming a crustal-confined *S*-wave splitting, our delay times would require an average anisotropy of 2.71%. This value is within the typical range of anisotropy percentage for crustal material, which has been estimated between 1.5 and 4% [*Savage,* 1999]. The largest values of seismic anisotropy percentage are present beneath stations PCON (4.74%), ANIL (4.37%), SOTA (2.97%) and POP2 (2.82%) (Table 3); these stations are located in the vicinity of active volcanoes, and the crustal anisotropy may be reflecting the presence of structures/fabrics product of deformational and volcanic processes that have been involved in the origin and

evolution of the Central Cordillera. Similarly, beneath stations ROSC and RUS, located in the Eastern Cordillera, the percentage of anisotropy also reaches considerable values (3.43 and 3.09%, respectively) (Table 3), which is indicative of complex fabrics product of the crustal shortening and uplift related to the genesis of this tectonically-inverted sedimentary basin.

Table 3. Crustal anisotropy percentage beneath the stations with local *S* splitting results. Crust thicknesses were taken from *Poveda et al.* [2015].

Station	Delay Time (s)	Crustal Thickness (km)	Crustal Anisotropy Percentage
ANIL	0.64	52.5	4.37
BRR	0.13	46.5	0.97
COD	0.11	35.5	1.14
PAL	0.19	35.0	1.93
PCON	0.63	47.5	4.74
POP2	0.26	33.5	2.82
ROSC	0.60	63.0	3.43
RUS	0.43	49.5	3.09
SOTA	0.46	56.0	2.97
TAM	0.26	41.0	2.30
URI	0.24	27.0	3.17
YOT	0.16	36.0	1.63

6.2 Lateral Variations of Subduction Geometry from *S*-wave Splitting Patterns

The northwestern corner of South America is characterized by a complex tectonic configuration as a result of the convergence of several major plates and a number of tectonic blocks with contrasting ages, thicknesses, and geological nature. This fact has favored the presence of significant lateral variations in the geometry of the lithosphere-asthenosphere system and therefore in the subduction-related mantle structure and dynamics beneath this region. From our results, it is clear that the anisotropic structure underlying the study zone varies significantly (Figure 4), and that several regions with contrasting *SKS* splitting patterns can be differentiated, and therefore related to different subduction segments.

A pronounced change in the *SKS* fast directions (φ) is seen at ~5°N, with NW-SE oriented φ to the north (Region I), and more complex φ to the south until ~2.8ºN (Region II), where the tendencies vary between ENE-WSW and WNW-ESE. The transition between these two regions coincides nicely with the proposed trace of the so-called Caldas Tear, which according to *Vargas and Mann* [2013], corresponds to the boundary between two subducted slabs with different strikes and dip angles. To the north of Caldas Tear, our *SKS* fast directions are consistently aligned with the general strike of the flat subduction of the Caribbean plate and Panama arc beneath South America. Similarly, the *SKS* φ values to the south are perpendicular/oblique to the trench related to the subduction of the Nazca oceanic lithosphere beneath the South American continent. Furthermore, there is a sub-region between the Caldas Tear and ~7.8°N where the stations reported larger δt values (>0.8 s), suggesting more intense deformation processes in the mantle. This could be related to the tectonic coupling between the Panama arc and Caribbean plate in this sector, and the subsequent increase in the buoyancy of the lithospheric system, which has led to an underthrusting process, as has been suggested by some authors [*Pennington,*

1981; *Vargas and Mann,* 2013]. In contrast, to the northeast of this sub-region, only the oceanic lithosphere of the Caribbean is subducting beneath South America with a steeper dip angle of ~20° [*Pennington,* 1981], which is consistent with the more modest lag times (<0.8 s) measured. The transition between these two sub-regions of contrasting *δt* values would mark the northern boundary of the Panama arc. Based on our observations, this boundary would be located somewhere between the stations URE and MON, extending towards the southeast near the station BRR. The nature of this boundary is not well constrained yet, and more investigation has to be done to determine if it corresponds to another lithospheric tear or a wide transition zone between the Panama arc and the Caribbean plate.

At ~2.8°N, another change in the *SKS* splitting pattern is detected which is related to another variation in the subduction geometry. To the south of this latitude (Region III), we found some NE-SW-oriented *SKS φ* tendencies with significant delay times (for example, stations TUM, OTAV and FLO2), which are pretty consistent with the general dip direction of the Ecuador segment of the Nazca plate subduction proposed by *Pennington* [1981]. In this region, the oceanic Carnegie Ridge is colliding against South America, and its subducted continuation as a flat slab beneath the Andes of southwestern Colombia and northern Ecuador extends up to ~400 km from the trench [*Gutscher et al.,* 1999]. The northeastward tectonic escape of the North Andes block relative to South America, as measured from GPS [*Trenkamp et al.,* 2002], has been related to the arrival of the Carnegie Ridge at the Colombia-Ecuador trench [*Pennington,* 1981; *Gutscher et al.,* 1999]. In this sense, our results suggest that an active flow in the asthenospheric mantle is driving the North Andes block to the northeast, and this flow continues to the north beneath the Eastern Cordillera and Merida Andes (as registered at stations ROSC, CHI, TAM, RUS, and SDV). The boundary between Regions II and III could be represented by a lithospheric tear, as it was suggested by *Gutscher et al.* [1999]. This feature, named here as Malpelo Tear, correspond to a wide anomalous zone with a probable NW-SE trend, localized between ~3.8°N and ~2.5°N where it reaches the Pacific coast of Colombia (Figure 7). This structure could be the expression of the subducted portion of the Malpelo Rift, which activity ceased ~8 Ma ago [*Hardy,* 1991; *Lonsdale and Klitgord,* 1978]. The *SKS* splitting observations along this tearing structure (stations MARA, POP2, PCON, and SOTA) are highly variable over very short distances, indicating a complicated underlying mantle structure and dynamics. Moreover, there are other geological and geophysical observations that account for the slab tearing beneath southwestern Colombia. First, several occurrences of alkaline volcanism reported between ~1.7°N and ~2.2°N [*Borrero and Castillo,* 2006] support the presence of a lithospheric-scale structural feature, like a slab tear, that allowed the rise of asthenospheric mantle material to the surface to produce this OIB-type volcanism in a typical scenario of slab window. Second, a clear change in the seismicity behavior is observed around ~3.4°N, where the occurrence of intermediate-to-deep earthquakes (>75 km) decreases dramatically to the south of this latitude, probably as a consequence of a shallower subduction angle; also there is a considerable reduction in the Quaternary calc-alkaline arc-related volcanic activity in this area. Finally, some significant breaks and possible offsets of regional gravity anomalies are clearly observed in the Malpelo Tear zone, which support the existence of this lithospheric discontinuity (Figure 7).
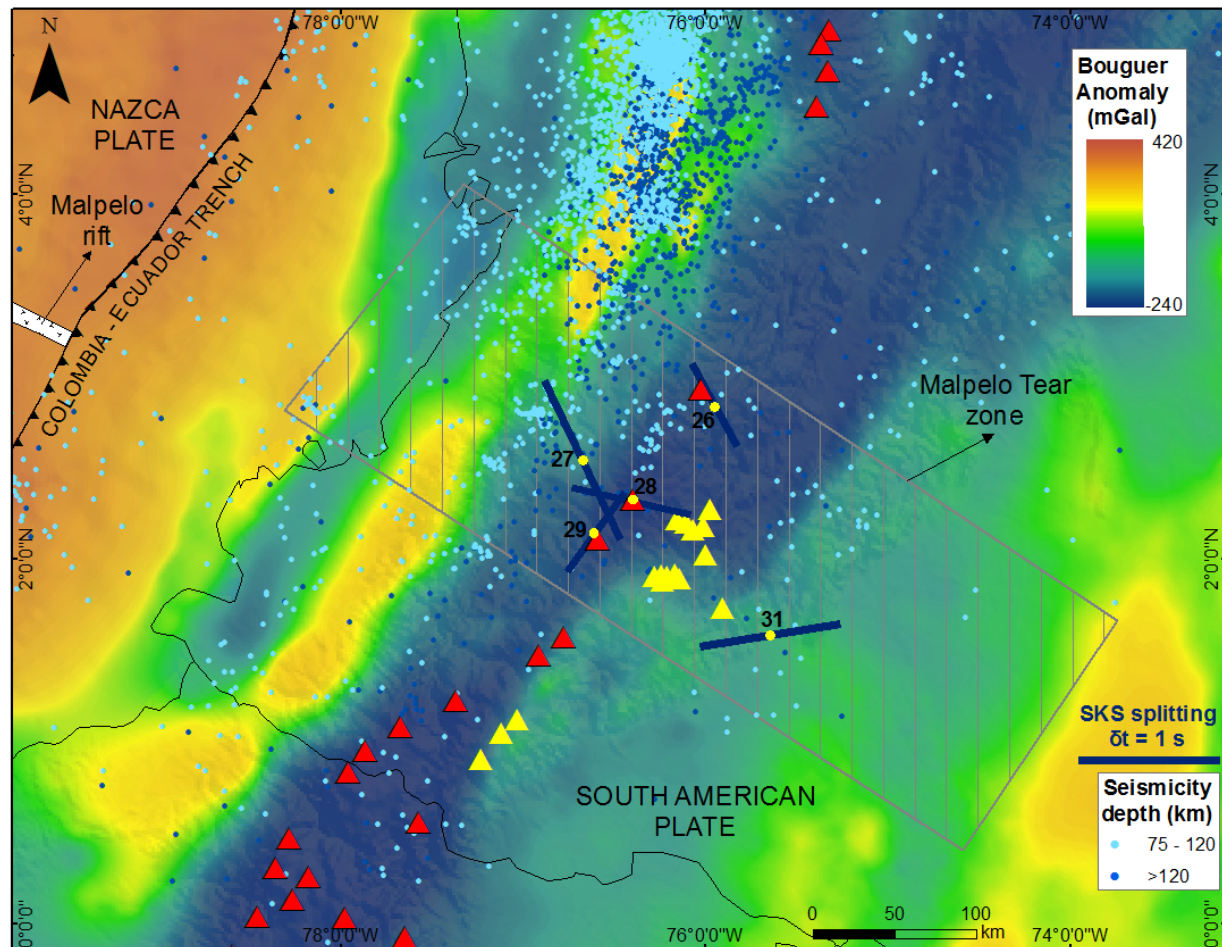
Figure 7. Malpelo Tear anomalous zone (gray polygon) in southwestern Colombia (see Figure 4 for location of this area). Disturbances in regional gravity anomalies (breaks and possible offsets), decrease in both intermediate-to-deep seismicity (blue dots) and calc-alkaline arc-related volcanism (red triangles), presence of OIB-type volcanism (yellow triangles), and highly variable *SKS* splitting (blue bars) behavior are evidences that account for the existence of this lithospheric structure. Bouguer anomalies data are taken from the WGM2012 global grid [*Bonvalot et al.,* 2012]. Seismic stations (yellow dots) numbers correspond to those listed in Table 1.

The regional distribution of the *SKS* splitting delay times also supports the lateral variations in the subduction geometries. Figure 8 shows the variation in the δt values along a profile oriented between N-S and NE-SW, roughly perpendicular to the subduction directions. North of ~7.8ºN, where the Caribbean plate is subducting beneath South America, the delay times are consistently small (<0.8 s) and exhibit a clear increase to the south, with values between 1.3 and 2.1 s. This change in the strength of the anisotropy is product of the current underthrusting of the coupled Panama Arc/Caribbean plate, which implies a sub-slab anisotropy layer nearly horizontal and more intensively deformed. Between Caldas and Malpelo tears (~5.5ºN and ~2.8ºN), the Nazca plate is descending beneath South America at a dip angle of ~35º. The steep downwelling asthenospheric flow product of this subduction angle results in weak splitting, as it is confirmed by the δt values obtained (between 0.4 and 1 s). Finally, south of Malpelo Tear, the flat subduction of the Carnegie Ridge beneath southwestern Colombia and northern Ecuador causes the increase in the anisotropy strength as it is evidenced by delay times around ~2 s.

6.3 Linking the Seismic Anisotropy to the Geodynamics of Northwestern South America

The nature of the mantle flow-field associated with subduction zones has been vigorously debated in the last years, and no global picture has been established yet. According to the compilations made by *Long and Silver* [2008, 2009] and *Long* [2013] on the relation between subduction geodynamics and seismic anisotropy, the sub-slab mantle shows splitting patterns that are, in general, simpler than those in the mantle above subducting slabs. Sub-slab mantle splitting studies have reported both trench-perpendicular and trench-parallel fast directions, with the latter behavior being the dominant in the global data set [*Long*, 2013]. Exceptions to this behavior (i.e. trench-normal φ) include Cascadia [*Currie et al.*, 2004], Mexico [*León-Soto et al.*, 2009], Greece [*Olive et al.*, 2011], and some sectors along South America [*Polet et al.*, 2000; *Porritt et al.*, 2014; *Eakin et al.*, 2015]. As it has been already described in the results section, our *SKS* fast directions are clearly trench-normal in the Region I, where the Caribbean plate and Panama arc are underthrusting northwestern South America. Our first interpretation is that these fast directions are roughly parallel to the local sub-slab mantle flow direction (Figures 9 and 10). This is supported by experiments on mineral physics which have evidenced that A-, C-, or E-type olivine fabrics are dominant in the mantle beneath subducting slabs, and that the conditions for the development of B-type fabric are absent in this environment [*Jung and Karato*, 2001; *Karato et al.*, 2008]. *SKS* fast directions are approximately parallel to the current velocity vector of the Caribbean plate [as reported by *Calais and Mann*, 2009; *Trenkamp et al.*, 2002], which suggests that the anisotropic structure could be related to lattice-preferred orientation (LPO) in the mantle beneath the subducting slab of the Caribbean, as a result of plate motion-related deformation and mechanical coupling between the descending slab and the upper mantle beneath it (Figures 9 and 10).

To the south, in Region II, *SKS* splitting φ orientations exhibit tendencies that are roughly parallel-subparallel to the motion vectors reported for the Nazca-South American plates convergence [*Calais and Mann*, 2009; *Trenkamp et al.*, 2002]. This would imply that the entrained mantle flow and deformation beneath the subducting Nazca slab are the main responsible for the measured *SKS* anisotropic signal (Figures 9 and 10). In the same way, the *SKS* splitting observations in Region III, although more complicated, show that most of the φ values are oriented NE-SW, therefore being parallel-subparallel to the convergence of the Carnegie Ridge against South America (Figure 10). This NE-SW-oriented mantle flow continues farther inland, in the Eastern Cordillera of Colombia and Merida Andes in Venezuela (Region IV), and is likely related to the northeastward movement of the North Andes block with respect to South America (Figure 10).
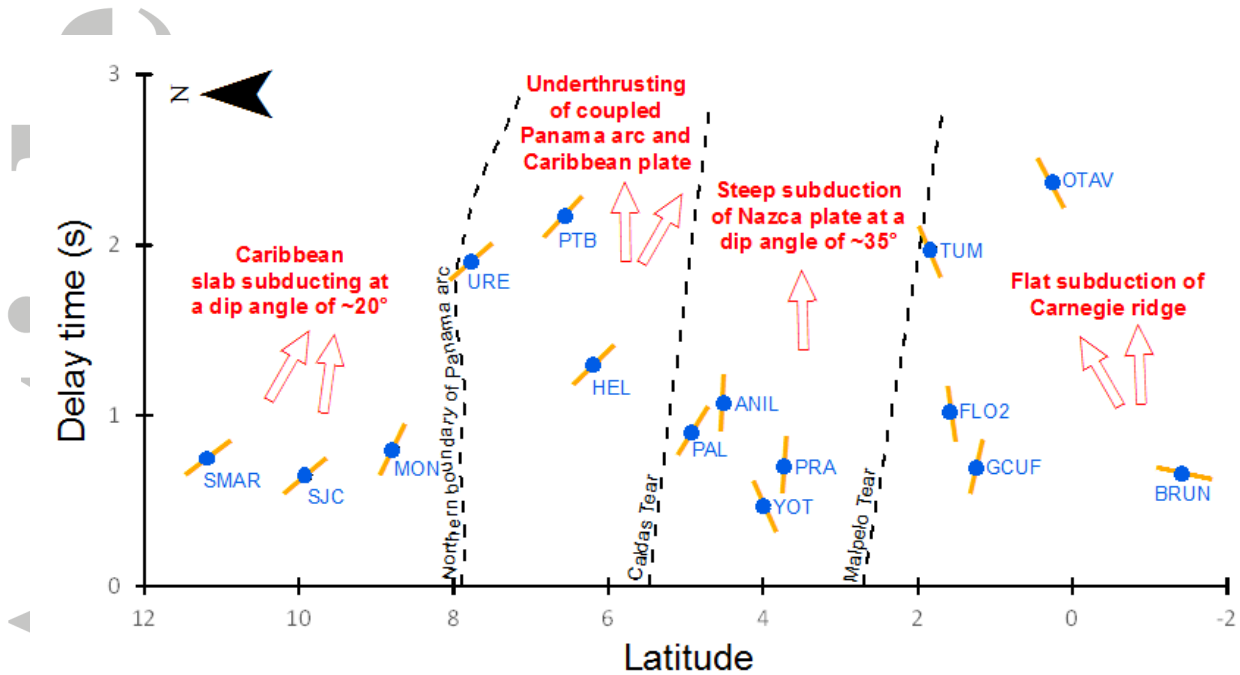
Figure 8. Variation of the *SKS* splitting delay times (blue dots represent the subset of *SKS* splitting results with the respective station name) across the different subduction segments. Larger *δt* values are associated with segments where very flat subduction or underthrusting is operating, and smaller *δt* values are observed in areas of steeper subduction angle. Also is shown the *SKS* fast direction (orange bars) and GPS vectors (open red arrows) [from *Trenkamp et al.,* 2002].

On the other hand, the splitting of the local *S* phase, according to its raypath, would sample the anisotropic fabric present in the mantle above the subducting slab (mantle wedge), and the overriding continental plate as well. Unfortunately, in this study we had a poor depth distribution of local earthquakes (90% of them are concentrated between 140 and 160 km), so constraining the source of the anisotropy is difficult. However, the observation that the fast directions are consistently aligned with the major fault systems in the area (Figure 5) could let us to hypothesize that the local splitting would be reflecting the anisotropic structure in the overriding South American continental crust or lithosphere, and that the mantle wedge would not be contributing notably to the measured splitting. Similar observations on the presence of largely isotropic mantle wedge have been reported in New Zealand [*Morley et al.,* 2006], Java-Sumatra [*Hammond et al.,* 2010], Indonesia-Philippine region [*Di Leo et al.,* 2012], the Caribbean [*Piñero-Feliciangeli and Kendall,* 2008], and South America [*Polet et al.,* 2000]. The reason of this apparent isotropy could be related to the fact that deformational processes in the mantle wedge, due to corner flow, are not strong enough to develop coherent lattice-preferred orientation (LPO) of olivine crystals [*Di Leo et al.,* 2012].
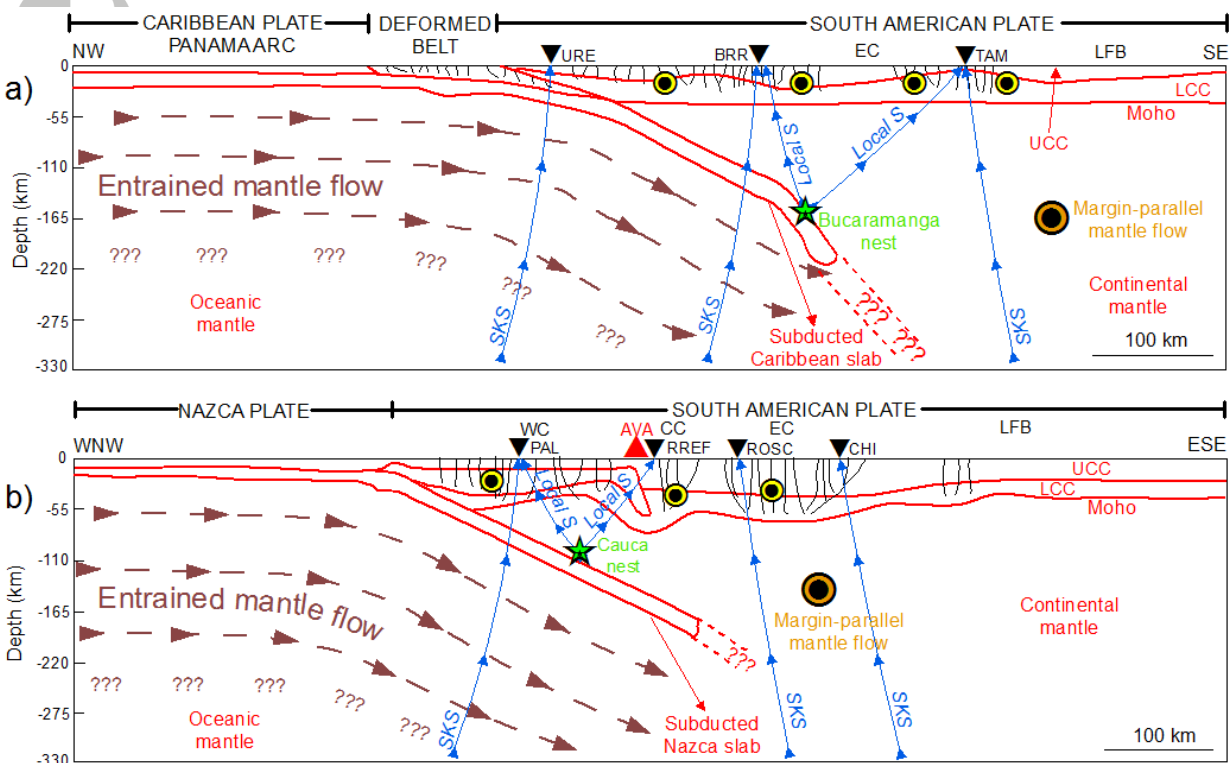
Figure 9. Regional sections showing the general interpretation of the *S*-wave splitting results north and south of the Caldas Tear. a) and b) correspond to the profiles AA' and BB' respectively in Figure 4. The ongoing underthrusting of the coupled Panama arc/Caribbean plate to the north of Caldas Tear is responsible for a strong *SKS* splitting signal beneath the descending slab by means of entrained mantle flow parallel to the direction of subduction. Similarly, south of Caldas Tear, the *SKS* anisotropy is reflecting a mechanical coupling between the descending Nazca slab and the mantle beneath it, but in this case, the splitting signal is weaker due to the steeper subduction angle. Further inland, there is an asthenospheric flow that is parallel to Pacific and Caribbean continental margins (orange/black circle) and is probably related to the northeastward motion of the North Andes block. Local *S* splitting appears to be strongly controlled by crustal-scale fault zones (bold black lines), therefore the anisotropy signal would be restricted to the continental crust (yellow/black circle). Finally, the mantle wedge is interpreted as apparently isotropic. Inverted black triangles are stations, and the red triangle indicates the location of the active volcanic arc (AVA). Blue arrows show the trajectories of *SKS* and local *S* phases. UCC: Upper Continental Crust; LCC: Lower Continental Crust; LFB: Llanos Foreland Basin; WC: Western Cordillera; CC: Central Cordillera; EC: Eastern Cordillera.

Finally, *Russo and Silver* [1994] proposed the presence of a horizontal trench-parallel flow in the mantle beneath the Nazca plate along the Andean continental margin, which passes into the Caribbean basin. It is evident that our results do not fit this continental-scale coast-parallel flow model, as we have presented here strong evidence for a trench-oblique to trench-perpendicular sub-slab entrained flow in both Nazca and Caribbean subduction zones. However, our *SKS* splitting measurements supports the existence of an asthenospheric mantle flow with significant delay times (1.0 to 1.7 s) that runs in a NE-SW direction beneath the stations located in the Eastern Cordillera of Colombia (stations CHI, ROSC, RUS, and TAM) and Merida Andes of Venezuela (station SDV). According to this, we hypothesize that the ongoing shallow subduction of the Carnegie Ridge in southwestern Colombia and northern Ecuador could have acted as a barrier and deflected *Russo and Silver's* [1994] flow further within the continent to continue in a NE-SW direction beneath Eastern Cordillera and Merida Andes. The same process may be

occurring along the distal area of the Panama arc indenter, on the Eastern Cordillera and northeast of the Caldas Tear. However, this hypothesis should be investigated more deeply, with the incorporation of geodynamical and mantle flow modeling.
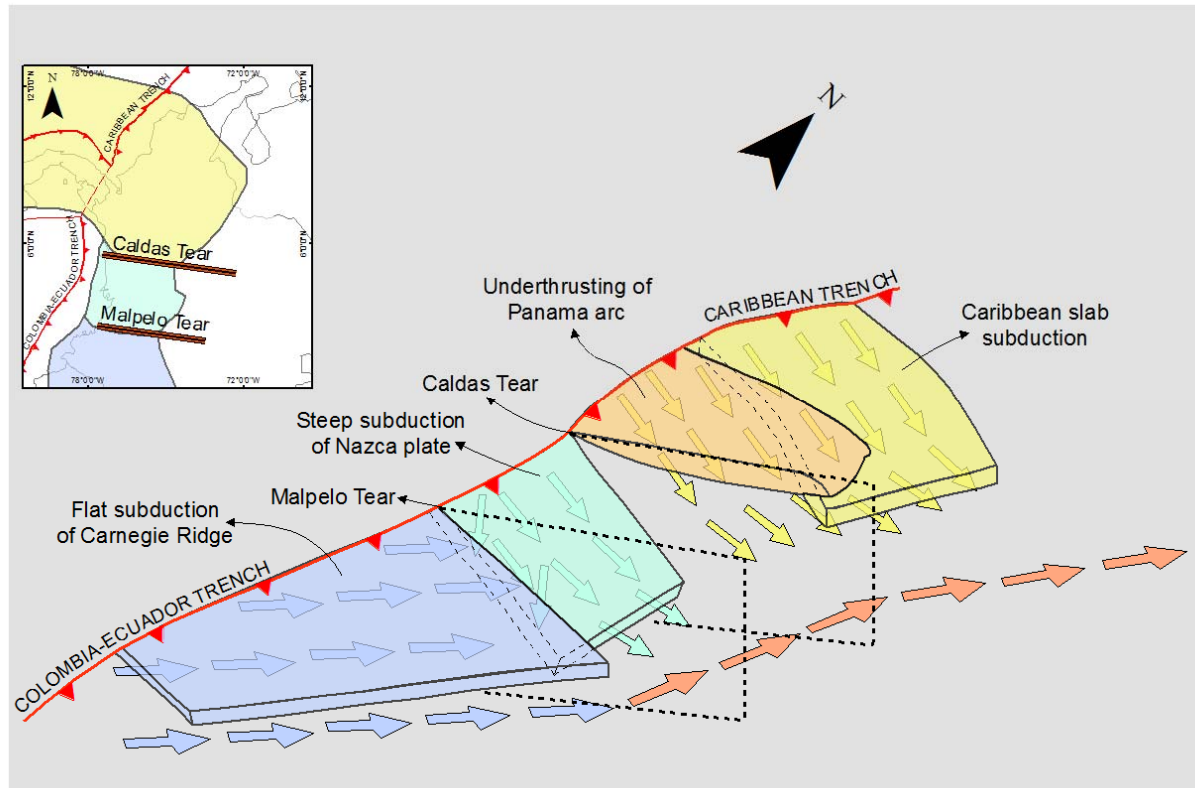

Figure 10. 3-D sketch of the geodynamic configuration of the different subduction segments in northwestern South America and the sub-slab asthenospheric flow patterns determined from *SKS* splitting. Two lithosphere-scale discontinuities, the Caldas Tear [*Vargas and Mann,* 2013] and Malpelo Tear (proposed in this study) are acting as the boundaries between slabs showing different subduction strikes and dip angles. Note the deflection to the northeast of the Caribbean sub-slab mantle flow (indicated by arrows with the color according to the corresponding subduction segment) caused by the presence of the Caldas Tear. Also, it is striking the complicated asthenospheric flow pattern around the Malpelo Tear, and the prolongation to the north of the NE-oriented flow related to the flat subduction of the Carnegie Ridge (blue arrows) beneath of Eastern Cordillera of Colombia and Merida Andes of Venezuela (orange arrows).

7 Conclusions

We have characterized the seismic anisotropy structure beneath northwestern South America from teleseismic *SKS* and local *S* splitting measurements. Our results clearly show that a significant and highly variable anisotropic fabric is present across the study area, and support the presence of several subduction segments with contrasting geometries and geodynamics bounded by lithospheric-scale tearing structures. The key finding of our investigation is that two distinct sources of *S*-wave anisotropy were detected: one located within the overriding continental crust of South America, and the other one located below the Caribbean and Nazca subducting slabs. Additionally, our observations argue that the mantle wedge does not contribute significantly to

the observed splitting. The range of delay times (δt) in the local S splitting (between 0.11 and 0.64 s) supports a continental crust-related seismic anisotropy, and the fact that most of the fast directions (φ) are oriented parallel-subparallel to a number of major fault systems suports this interpretation. On the other hand, SKS splitting reveals evidence of asthenospheric flow beneath the downgoing oceanic slabs that is parallel-subparallel to the subduction dip direction; this observation accounts for an entrained mantle flow product of a high mechanical coupling between the slabs and the asthenospheric material below them. Striking lateral variations in the SKS splitting parameters (φ and δt) observed along the study zone provide a coherent picture of the changes in the subduction geometries, from flat- (underthrusting) to steep-angle, where the transition zones between the different segments are marked by lithospheric tears (Caldas and Malpelo tears). Furthermore, it seems that the sub-slab mantle flow patterns are highly controlled by the presence of these tearing structures, as it can be seen around the Caldas Tear where the mantle flow beneath the subducting Caribbean slab is deflected to the east-northeast, and continue beneath Eastern Cordillera and Merida Andes. The results presented in this paper contribute to the understanding of the complex geodynamic setting currently operating in the northwestern corner of South America and provide new insights into the anisotropic fabrics present in subduction zones.

Acknowledgments and Supporting Data

Readers can find in the Supporting Information section the Table S1, which includes the description of all the S-wave splitting measurements obtained in this study, and Figures S1, S2 and S3 including the individual measurements of the SKS and local S splitting, and the variation of the SKS splitting parameters with backazimuth.

References

Alsina, D., and R. Sneider (1995), Small-scale sublithospheric continental mantle deformation: constraints from SKS splitting observations, Geophys. J. Int., 123(2), 431-448, doi: 10.1111/j.1365-246X.1995.tb06864.x.

Audemard, F. (1993), Néotectonique, sismotectonique et aléa sismique du Nord-ouest du Vénézuéla (Système de failles d'Oca- Ancón). PhD thesis, Université Montpellier II. France, 369 pp + Appendix.

Backus, G. E. (1962), Long-wave elastic anisotropy produced by horizontal layering, J. Geophys. Res., 67, 4427-4440, doi: 10.1029/JZ067i011p04427.

Bernal-Olaya, R., C. A. Vargas, and P. Mann (2015), Earthquake, tomographic, seismic reflection, and gravity evidence for a shallowly dipping subduction zone beneath the Caribbean margin of northwestern Colombia, In: C. Bartolini and P. Mann. (Eds.), Petroleum geology and potential of the Colombian Caribbean margin, AAPG Memoir, 108, 247-270, doi: 10.1306/13531939M1083642.

Bonvalot, S., G. Balmino, A. Briais, M. Kuhn, A. Peyrefitte, N. Vales, R. Biancale, G. Gabalda, F. Reinquin, and M. Sarrailh (2012), World Gravity Map. Commission for the Geological Map of the World. Eds. BGI-CGMW-CNES-IRD, Paris.

Borrero, C. A., and H. Castillo (2006), Vulcanitas del S-SE de Colombia: Retro-arco alcalino y su posible relación con una ventana astenosférica, Boletín de Geología, 28(2), 23-34.

Calais, E., and P. Mann (2009), A combined GPS velocity field for the Caribbean plate and its margins (abstract #G33B-0657), American Geophysical Union, (Fall Meet.), G33B-0657.

Corredor, F. (2003), Seismic strain rates and distributed continental deformation in the northern Andes and three-dimensional seismotectonics of northwestern South America, Tectonophysics, 372, 147-166, doi:10.1016/S0040-1951(03)00276-2.

Cortés, M., and J. Angelier (2005), Current states of stress in the northern Andes as indicated by focal mechanisms of earthquakes, Tectonophysics, 403, 29-58, doi:10.1016/j.tecto.2005.03.020.

Crampin, S., and D. C. Booth (1985), Shear-wave polarizations near the North Anatolian Fault II, Interpretation in terms of crack-induced anisotropy, Geophys. J. R. Astron. Soc., 83(1), 75-92, doi: 10.1111/j.1365-246X.1985.tb05157.x.

Currie, C. A., J. F. Cassidy, R. D. Hyndman, and M. G. Bostock (2004), Shear wave anisotropy beneath the Cascadia subduction zone and western North American craton, Geophys. J. Int., 157(1), 341-353, doi: 10.1111/j.1365-246X.2004.02175.x.

Di Leo, J. F., J. Wookey, J. O. S. Hammond, J. -M. Kendall, S. Kaneshima, H. Inoue, T. Yamashina, and P. Harjadi (2012), Deformation and mantle flow beneath the Sangihe subduction zone from seismic anisotropy, Phys. Earth Planet. Int., 194-195, 38-54, doi: 10.1016/j.pepi.2012.01.008.

Eakin, C. M., M. D. Long, L. S. Wagner, and S. L. Beck (2015), Upper mantle anisotropy beneath Peru from SKS splitting: Constraints on flat slab dynamics and interaction with the Nazca Ridge, Earth Planet. Sci. Let., 412, 152-162, doi:10.1016/j.epsl.2014.12.015.

Frohlich, C., K. Kadinsky-Cade, and S. D. Davis (1995), A reexamination of the Bucaramanga, Colombia, earthquake nest, Bull. Seismol. Soc. Am., 85(6), 1622-1634.

Gutscher, M. -A., J. Malavieille, S. Lallemand, and J. -Y Collot (1999), Tectonic segmentation of the North Andean margin: impact of the Carnegie Ridge collision, Earth Planet. Sci. Let., 168(3-4), 255-270, doi:10.1016/S0012-821X(99)00060-6.

Gutscher, M. -A., W. Spakman, H. Bijwaard, and E. R. Engdahl (2000), Geodynamics of flat subduction: Seismicity and tomographic constraints from the Andean margin, Tectonics, 19(5), 814-833.

Hammond, J. O. S., J. -M Kendall, D. Angus, J. and Wookey (2010), Interpreting spatial variations in anisotropy: Insights into the Main Ethiopian Rift from SKS waveform modelling, Geophys. J. Int., 181(3), 1701-1712, doi: 10.1111/j.1365-246X.2010.04587.x.

Hardy, N. C. (1991), Tectonic evolution of the easternmost Panama basin: Some new data and inferences, J. South Amer. Earth Sci., 4(3), 261-269, doi: 10.1016/0895-9811(91)90035-J.

Jung, H., and S. Karato (2001), Water-induced fabric transitions in olivine, Science, 293, 1460-1463, doi: 10.1126/science.1062235.

Kaneshima, S., and M. Ando (1989), An analysis of split shear waves observed above crustal and uppermost mantle earthquakes beneath Shikoku, Japan: Implications in effective depth extent of seismic anisotropy, J. Geophys. Res., 94(B10), 14077-14092, doi: 10.1029/JB094iB10p14077.

Karato, S., H. Jung, I, Katayama, and P., Skemer (2008), Geodynamic significance of seismic anisotropy of the upper mantle: new insights from laboratory studies, Annu. Rev. 36, 59-95, doi: 10.1146/annurev.earth.36.031207.124120.

Kendall, J. -M. (1994), Teleseismic arrivals at a mid-ocean ridge: Effect of mantle melt and anisotropy, Geophys. Res. Lett., 21(4), 301-304.

León Soto, G., J. F. Ni, S. P. Grand, E. Sandvol, R. W. Valenzuela, M. Guzmán Speziale, J. M. Gómez González, and T. Domínguez Reyes (2009), Mantle flow in the Rivera-Cocos subduction zone, Geophys. J. Int., 179(2), 1004-1012, doi:10.1111/j.1365-246X.2009.04352.x.

Levin, V., and J. Park (1998), P-SH conversions in layered media with hexagonally symmetric anisotropy: a cookbook, Pure Appl. Geophys., 151, 669-697, doi: 0033–4553/98/040669–29.

Long, M. D., and P. G. Silver (2008), The subduction zone flow field from seismic anisotropy: A global view, Science, 319(5861), 315-319, doi: 10.1126/science.1150809.

Long, M. D., and P. G. Silver (2009), Shear wave splitting and mantle anisotropy: Measurements, interpretations, and new directions, Surv. Geophys., 30, 407-461, doi: 10.1007/s10712-009-9075-1.

Long, M. D., and T. W. Becker (2010), Mantle dynamics and seismic anisotropy, Earth Planet. Sci. Lett., 297, 341-354, doi: 10.1016/j.epsl.2010.06.036.

Long, M. D. (2013), Constraints on subduction geodynamics from seismic anisotropy, Rev. Geophys., 51, 76-112, doi: 10.1002/rog.20008.

Lonsdale, P., and K. D. Klitgord (1978), Structure and tectonic history of the eastern Panama Basin, Bull. Geol. Soc. Am. 89(7), 981-999, doi: 10.1130/0016-7606.

Mainprice, D., and P. G. Silver (1993), Interpretation of SKS-waves using samples from the subcontinental lithosphere, Phys. Earth Planet. In., 78(3-4), 257-280, doi: 10.1016/0031-9201(93)90160-B.

Mainprice, D. (1997), Modelling the anisotropic seismic properties of partially molten rocks found at mid-ocean ridges, Tectonophysics, 279(1-4), 161-179, doi: 10.1016/S0040-1951(97)00122-4.

Mainprice D., A. Tommasi, H. Couvy, P. Cordier, and D. J. Frost (2005), Pressure sensitivity of olivine slip systems: implications for the interpretation of seismic anisotropy of the Earth's upper mantle, Nature 433, 731-733, doi: 10.1038/nature03266.

Masy, J., F. Niu, A. Levander, and M. Schmitz (2011), Mantle flow beneath northwestern Venezuela: Seismic evidence for a deep origin of the Mérida Andes, Earth Planet. Sci. Lett., 305(3-4), 396-404, doi: 10.1016/j.epsl.2011.03.024.

Morley, A. M., G. W. Stuart, J. -M. Kendall, and M. Reyners (2006), Mantle wedge anisotropy in the Hikurangi subduction zone, central North Island, New Zealand, Geophys. Res. Lett., 33(5), 1-4, doi: 10.1029/2005GL024569.

Olive, J. A., S. Rondenay, and F. Pearce (2011), Evidence for trench-normal flow beneath the Western Hellenic slab from shear-wave splitting analysis, Abstract DI41A-2067 presented at the AGU Fall Meeting.

Pennington, W. D. (1981), Subduction of the eastern Panama basin and seismotectonics of northwestern South America, J. Geophys. Res., 86(B11), 10753-10770, doi: 10.1029/JB086iB11p10753.

Piñero-Feliciangeli, L., and J. -M. Kendall (2008), Sub-slab mantle flow parallel to the Caribbean plate boundaries: Inferences from SKS splitting, Tectonophysics, 462(1-4), 22–34, doi: 10.1016/j.tecto.2008.01.022.

Polet, J., P. G. Silver, S. Beck, T. Wallace, G. Zandt, S. Ruppert, R. Kind, and A. Rudloff (2000), Shear wave anisotropy beneath the Andes from the BANJO, SEDA, and PISCO experiments, J. Geophys. Res., 105(B3), 6287-6304, doi: 10.1029/1999JB900326.

Porritt, R. W., T. W. Becker, and G. Monsalve (2014), Seismic anisotropy and slab dynamics from SKS splitting recorded in Colombia, Geophys. Res. Lett., 41, 8775-8783, doi: 10.1002/2014GL061958.

Poveda, E., G. Monsalve, and C. A. Vargas (2015), Receiver functions and crustal structure of the northwestern Andean region, Colombia, J. Geophys. Res. Solid Earth, 120(4), 2408-2425, doi: 10.1002/2014JB011304.

Restivo, A., and G. Helffrich (2006), Core-mantle boundary structure investigated using SKS and SKKS polarization anomalies, Geophys. J. Int., 165(1), 288-302, doi: 10.1111/j.1365-246X.2006.02901.x.

Russo, R. M., and P. G. Silver (1994), Trench-parallel flow beneath the Nazca plate from seismic anisotropy, Science, 263(5150), 1105-1111, doi: 10.1126/science.263.5150.1105.

Savage, M.K., W.A. Peppin, U.R. Vetter, 1990, Shear-wave anisotropy and stress direction in and near Long Valley Caldera, California, 1979-1988, J. Geophys. Res., 95, 11165-11177.

Savage, M. K. (1999), Seismic anisotropy and mantle deformation: What have we learned from shear wave splitting?, Rev. Geophys., 37(1), 65-106, doi: 10.1029/98RG02075.

Schneider, J. F., W. D. Pennington, and R. P. Meyer (1987), Microseismicity and focal mechanisms of the intermediate-depth Bucaramanga nest, Colombia, J. Geophys. Res., 92(B13), 13913-13926, doi: 10.1029/JB092iB13p13913.

Shih, X. R., J. F. Schneider, and R. P. Meyer (1991), Polarities of P and S waves, and shear wave splitting observed from the Bucaramanga nest, Colombia, J. Geophys. Res., 96, 12069-12082, doi: 10.1029/91JB01201.

Silver, P. G., and W. W. Chan (1991), Shear wave splitting and subcontinental mantle deformation, J. Geophys. Res., 96(B10), 16429-16454, doi: 10.1029/91JB00899.

Taboada, A., L. A. Rivera, A. Fuenzalida, A. Cisternas, H. Philip, H. Bijwaard, J. Olaya, and C. Rivera (2000), Geodynamics of the Northern Andes, subductions and intracontinental deformation (Colombia), Tectonics, 19, 787-813, doi: 10.1029/2000TC900004.

Teanby, N. A., J. -M. Kendall, and M. van der Baan (2004), Automation of shear-wave splitting measurements using cluster analysis, Bull. Seism. Soc. Am., 94(2), 453-463, doi: 10.1785/0120030123.

Trenkamp, R., J. N. Kellogg, J. T. Freymueller, and H. Mora (2002), Wide plate margin deformation, southern Central America and northwestern South America, CASA GPS observations, J. S. Am. Earth Sci., 15(2), 157-171.

van der Hilst, R. D., and P. Mann (1994), Tectonic implications of tomographic images of subducted lithosphere beneath northwestern South America, Geology, 22(5), 451-454, doi: 10.1130/0091-7613.

Vargas, C. A., and P. Mann (2013), Tearing and breaking off of subducted slabs as the result of collision of the Panama arc-indenter with Northwestern South America, Bull. Seismol. Soc. Am., 103(3), 2025-2046, doi: 10.1785/0120120328.